CONTINUOUS MANEUVERS FOR SPACECRAFT FORMATION FLYING RECONFIGURATION USING RELATIVE ORBIT ELEMENTS

G. Di Mauro,[*] R. Bevilacqua,[†] D. Spiller[‡], J. Sullivan[§] and S. D'Amico[**]

This paper presents the solutions to the spacecraft relative trajectory reconfiguration problem when a continuous thrust profile is used, and the reference orbit is circular. Given a continuous on/off thrust profile, the proposed approach enables the computation of the control solution by inverting the linearized equations of relative motion parameterized using the mean relative orbit elements. The use of mean relative orbit elements facilitates the inclusion of the Earth's oblateness effects and offers an immediate insight into the relative motion geometry. Several reconfiguration maneuvers are presented to show the effectiveness of the obtained control scheme.

INTRODUCTION

Spacecraft formation flying concepts have become a topic of interest in recent years given the associated benefits in terms of cost, mission flexibility/robustness, and enhanced performance[1,2]. Replacing a complex, monolithic spacecraft with an array of simpler and highly coordinated satellites increases the performance of interferometric instruments through the aperture synthesis. The configuration of formations can also be adjusted to compensate for malfunctioning vehicles without forcing a mission abort or be reconfigured to accomplish new tasks.

Among the various technical challenges involved in spacecraft formation flying, the reconfiguration problem represents a key aspect that has been intensively studied over the last years[2]. Formation reconfiguration pertains to the achievement of a specific relative orbit in a defined time interval given an initial formation configuration. So far, many methods have been proposed to solve the aforementioned problem, ranging from impulsive to continuous control techniques. Impulsive strategies have been widely investigated since they provide a closed-form solution to the relative motion control problem. Such solutions are generally based on 1) the use of the Gauss variational equations (GVE) to determine the control influence matrix, and 2) on the inversion of

---

[*] PostDoc Associate, Department of Mechanical & Aerospace Engineering, ADAMUS Laboratory, University of Florida, 939 Sweetwater Dr., Gainesville, FL 32611 – 6250.
[†] Associate Professor, Department of Mechanical & Aerospace Engineering, ADAMUS Laboratory, University of Florida, 939 Sweetwater Dr., Gainesville, FL 32611 – 6250. AIAA Senior Member.
[‡] PhD candidate, Department of Aerospace and Mechanical Engineering, Sapienza University of Rome, via Eudossiana 18, 00100.
[§] PhD Candidate, Stanford University, Department of Aeronautics and Astronautics, Space Rendezvous Laboratory, Durand Building, 496 Lomita Mall, Stanford, CA 94305-4035.
[**] Assistant Professor, Department of Aeronautics and Astronautics Engineering, Stanford's Space Rendezvous Lab, Stanford University, 496 Lomita Mall, Stanford, CA 94305-4035.

the state transition matrix (STM) associated with a set of linear equations of relative motion. In (Reference 1) the authors addressed the issues of establishing and reconfiguring a multi-spacecraft formation consisting of a central chief satellite surrounded by four deputy spacecraft using impulsive control under the assumption of two-body orbital mechanics. They proposed an analytical two-impulse control scheme for transferring a deputy spacecraft from a given location in the initial configuration to any given final configuration using the GVE. Ichimura and Ichikawa developed an analytical open-time minimum fuel impulsive strategy associated with the Hill-Clohessy-Wiltshire equations of relative motion. The approach involves three in-plane impulses to achieve the optimal in-plane reconfiguration[2]. Chernick *et al.* addressed the computation of fuel-optimal control solutions for formation reconfiguration using impulsive maneuvers. They developed semi-analytical solutions for in-plane and out-of-plane reconfigurations in near-circular J_2-perturbed and eccentric unperturbed orbits, using the relative orbit elements (ROE) to parameterize the equations of relative motion[3]. More recently, Lawn *et al.* proposed a continuous low-thrust strategy based on the input-shaping technique for the short-distance planar spacecraft rephasing and rendezvous maneuvering problems. The analytical solution was obtained by exploiting the Schweighart and Sedwick (SS) linear dynamics model[4]. A continuous low-thrust control strategy for formations operating in perturbed orbits of arbitrary eccentricity was also proposed by Steindorf *et al.* They derived a control law for the mean ROE based on the Lyapunov theory and implemented guidance algorithms based on potential fields. This approach allowed time constraints, thrust level constraints, wall constraints, and passive collision avoidance constraints to be included in the guidance strategy[5].

Additionally, the growing use of small spacecraft for formation flying missions poses new challenges for reconfiguration maneuvering. Due to the vehicles' limited size and on-board power, small spacecraft are typically equipped with small thrusters which only operate in on/off configurations to deliver low thrust. Additionally, these platforms often have limited computing capabilities which necessitate analytical formation control algorithms that are designed to avoid computationally burdensome numerical methods while computing maneuvers that are compliant with the thrust profile constraints.

In light of the above challenges, the main contributions of this work are:

- the development of a linearized relative dynamics model which accounts for the J_2 perturbation and control accelerations in circular reference orbits. The corresponding closed-form solution developed in this work extends the results previously published in (Reference 6) by computing the input matrix and the corresponding convolution matrix;

- the derivation of the analytical and semi-analytical solutions for the in-plane and out-of-plane formation reconfiguration maneuvering problems using an on/off continuous thrust profile. In further details, the impulsive maneuver strategy presented in (Reference 3) is reformulated to include the effects of a finite duration thrust profile, in order to enhance the maneuver accuracy.

The rest of the paper is organized as follows. In the first section, the differential equations (and their associated linearization) describing the relative motion of two Earth orbiting spacecraft under the effects of J_2 and continuous external accelerations are presented. A closed-form solution for the linearized relative motion is determined for near-circular J_2-perturbed orbit cases, i.e. for very small or zero eccentricity. The subsequent section is dedicated to the derivation of solutions for the in-plane, out-of-plane and full spacecraft formation reconfiguration problems. The final section shows the relative trajectories obtained using the developed control solutions, pointing out their performances in terms of maneuver cost and accuracy. Having fixed the total number

of maneuvers, the derived analytical and semi-analytical solutions are compared with the numerical ones obtained using a Matlab optimizer.

RELATIVE DYNAMICS MODEL

In this section the dynamics model used to describe the relative motion between two spacecraft orbiting the Earth is presented. The model is formalized by using the ROE state as defined by D'Amico in (Reference 7), and allows for the inclusion of Earth oblateness J_2 and external constant acceleration effects.

Relative Orbit Elements

The absolute orbit of a satellite can be expressed by the set of classical Keplerian orbit elements, $\boldsymbol{\alpha} = [a, e, i, \omega, \Omega, M]^T$. The relative motion of a *deputy* spacecraft with respect to another one, referred to as *chief*, can be parameterized using the dimensionless relative orbit elements defined in (Reference 7) and here recalled for completeness,

$$\delta\boldsymbol{\alpha} = \begin{bmatrix} \dfrac{a_d}{a_c} - 1 \\ (M_d - M_c) + (\omega_d - \omega_c) + (\Omega_d - \Omega_c)c_{i_c} \\ e_{xd} - e_{xc} \\ e_{yd} - e_{yc} \\ i_d - i_c \\ (\Omega_d - \Omega_c)s_{i_c} \end{bmatrix} = \begin{bmatrix} \delta a \\ \delta\lambda \\ \delta e_x \\ \delta e_y \\ \delta i_x \\ \delta i_y \end{bmatrix} \tag{1}$$

In Eq. (1) the subscripts "c" and "d" label the chief and deputy satellites respectively, whereas $s_{(.)} = sin()$ and $c_{(.)} = cos()$. Moreover, $e_{x(\cdot)} = e_{(\cdot)}c_{\omega_{(\cdot)}}$ and $e_{y(\cdot)} = e_{(\cdot)}s_{\omega_{(\cdot)}}$ are defined as the components of the eccentricity vector and ω is the argument of perigee. The first two components of the relative state, $\delta\boldsymbol{\alpha}$, are the relative semi-major axis, δa, and the relative mean longitude $\delta\lambda$, whereas the remaining components constitute the coordinates of the relative eccentricity vector, $\delta\boldsymbol{e}$, and relative inclination vector, $\delta\boldsymbol{i}$. It is worth remarking that the use of the ROE parameterization facilitates the inclusion of perturbing accelerations such as Earth oblateness J_2 effects or atmospheric drag into the dynamical model[6] and offers an immediate insight into the relative motion geometry[8]. In addition, the above relative state is non-singular for circular orbits ($e_c = 0$), whereas it is still singular for strictly equatorial orbits ($i_c = 0$).

Non-linear Equations of Relative Motion

The averaged variations of mean ROE (i.e. without short- and long-periodic terms) caused by the Earth's oblateness J_2 effects can be derived from the differentiation of chief and deputy mean classical elements (see Reference 6 and 11), $\boldsymbol{\alpha}_c = [a_c, e_c, i_c, \omega_c, \Omega_c, M_c]^T$ and $\boldsymbol{\alpha}_d = [a_d, e_d, i_d, \omega_d, \Omega_d, M_d]^T$ respectively,

$$\dot{\boldsymbol{\alpha}}_{c,J2} = \begin{bmatrix} \dot{a}_c \\ \dot{e}_c \\ \dot{i}_c \\ \dot{\omega}_c \\ \dot{\Omega}_c \\ \dot{M}_c \end{bmatrix} = K_c \begin{bmatrix} \mathbf{0}_{3x1} \\ Q_c \\ -2\cos(i_c) \\ \eta_c P_c \end{bmatrix} \quad \dot{\boldsymbol{\alpha}}_{d,J2} = \begin{bmatrix} \dot{a}_d \\ \dot{e}_d \\ \dot{i}_d \\ \dot{\omega}_d \\ \dot{\Omega}_d \\ \dot{M}_d \end{bmatrix} = K_d \begin{bmatrix} \mathbf{0}_{3x1} \\ Q_d \\ -2\cos(i_d) \\ \eta_d P_d \end{bmatrix}, \tag{2}$$

where

$$K_j = \frac{\gamma n_j}{a_j^2 \eta_j^4} \qquad \eta_j = \sqrt{1 - e_j^2} \qquad n_j = \sqrt{\frac{\mu}{a_j^3}}$$

$$Q_j = 5\cos(i_j)^2 - 1 \quad P_j = 3\cos(i_j)^2 - 1 \quad \gamma = \frac{3}{4}J_2 R_E^2 \tag{3}$$

In Eq. (3) the subscript "j" stands for "c" and "d". J_2 indicates the second spherical harmonic of the Earth's geopotential, R_E the Earth's equatorial radius and μ the Earth gravitational parameter. Computing the time derivative of mean ROE as defined in Eq. (1) and substituting Eq. (2) yields

$$\delta\dot{\boldsymbol{\alpha}}_{J2} = \begin{bmatrix} 0 \\ \dot{M}_d - \dot{M}_c - (\dot{\omega}_d - \dot{\omega}_c) + (\dot{\Omega}_d - \dot{\Omega}_c)c_{i_c} \\ -e_d s_{\omega_d}\dot{\omega}_d + e_c s_{\omega_c}\dot{\omega}_c \\ +e_d c_{\omega_d}\dot{\omega}_d - e_c c_{\omega_c}\dot{\omega}_c \\ 0 \\ (\dot{\Omega}_d - \dot{\Omega}_c)s_{i_c} \end{bmatrix} = \boldsymbol{\sigma}_{J2}(\boldsymbol{\alpha}_c, \boldsymbol{\alpha}_d) \tag{4}$$

with

$$\boldsymbol{\sigma}_{J2}(\boldsymbol{\alpha}_c, \boldsymbol{\alpha}_d) = \begin{bmatrix} 0 \\ (\eta_d P_d K_d - \eta_c P_c K_c) + (K_d Q_d - K_c Q_c) - 2(K_d c_{i_d} - K_c c_{i_c})c_{i_c} \\ -e_{yd}K_d Q_d + e_{yc}K_c Q_c \\ e_{xd}K_d Q_d - e_{xc}K_c Q_c \\ 0 \\ -2(K_d c_{i_d} - K_c c_{i_c})s_{i_c} \end{bmatrix} \tag{5}$$

In this study only the deputy is assumed to be maneuverable and capable of providing continuous thrust along x, y, and z directions of its own Local Vertical Local Horizontal (LVLH) reference frame. The LVLH frame consists of orthogonal basis vectors with x pointing along the deputy absolute radius vector, z pointing along the angular momentum vector of the deputy absolute orbit, and $y = z \times x$ completing the triad and pointing in the along-track direction. The change of mean ROE caused by a continuous control acceleration vector $\boldsymbol{F}$ can be determined through the well-known Gauss variational equations (GVE)[9,10]. In fact, as widely discussed in (Reference 10), the mean orbit elements can be reasonably approximated by the corresponding osculating elements since the Jacobian of the osculating-to-mean transformation is approximately a 6x6 identity matrix, with the off-diagonal terms being of order J_2 or smaller. In other words, the variations of osculating elements are directly reflected in corresponding mean orbit elements changes. In light of the above, the variation of mean ROE induced by the external force is

$$\delta\dot{\boldsymbol{\alpha}}_F = \begin{bmatrix} \dfrac{\dot{a}_d}{a_c} \\ (\dot{M}_d) + (\dot{\omega}_d) + (\dot{\Omega}_d)c_{i_c} \\ \dot{e}_d c_{\omega_d} - e_d s_{\omega_d}\dot{\omega}_d \\ \dot{e}_d s_{\omega_d} + e_d c_{\omega_d}\dot{\omega}_d \\ \dot{i}_d \\ (\dot{\Omega}_d)s_{i_c} \end{bmatrix} = \boldsymbol{\sigma}_F(\boldsymbol{\alpha}_d, \boldsymbol{F}) = \boldsymbol{\Gamma}_F(\boldsymbol{\alpha}_d)\boldsymbol{F}, \tag{6}$$

where the control acceleration vector F is expressed in the spacecraft LVLH frame components as $F = [f_x, f_y, f_z]^T$. The individual terms of the control influence matrix Γ_F are reported in Appendix A.

The relative motion between the deputy and chief satellites is given by adding the contributions from Keplerian gravity, the J_2 perturbation, and the external force vector F. The final set of nonlinear differential equations is

$$\delta\dot{\alpha} = [0, n_d - n_c, 0,0,0,0]^T + \sigma_{J2}(\alpha_c, \alpha_d) + \sigma_F(\alpha_d, F) = \xi(\alpha_c, \alpha_d(\alpha_c, \delta\alpha), F) \tag{7}$$

Note that the function $\xi(\alpha_c, \alpha_d(\alpha_c, \delta\alpha), F)$ can be reformulated in terms of α_c and $\delta\alpha$ using the following identities,

$$a_d = a_c\delta a + a_c \qquad \Omega_d = \Omega_c + \frac{\delta i_y}{s_{i_c}} \qquad e_d = \sqrt{\left(e_c c_{\omega_c} + \delta e_x\right)^2 + \left(e_c s_{\omega_c} + \delta e_y\right)^2}$$

$$i_d = i_c + \delta i_x \qquad \omega_d = \tan^{-1}\left(\frac{e_c s_{\omega_c} + \delta e_y}{e_c c_{\omega_c} + \delta e_x}\right) \qquad M_d = M_c + \delta\lambda - (\omega_d - \omega_c) - (\Omega_d - \Omega_c)c_{i_c} \tag{8}$$

such that $\delta\dot{\alpha} = \xi(\alpha_c, \delta\alpha, F)$.

Linearized Equations of Relative Motion

In order to obtain the linearized equations of relative motion, $\delta\dot{\alpha}$ in Eq. (7) can be expanded about the chief orbit (i.e., $\delta\alpha = 0$ and $F = 0$) to first order using a Taylor expansion,

$$\delta\dot{\alpha}(t) = \frac{\partial\xi}{\partial\delta\alpha}\bigg|_{\substack{\delta\alpha=0 \\ F=0}} \delta\alpha(t) + \frac{\partial\xi}{\partial F}\bigg|_{\substack{\delta\alpha=0 \\ F=0}} F = A(\alpha_c(t))\,\delta\alpha(t) + B(\alpha_c(t))F. \tag{9}$$

The matrices A and B represent the plant and input matrices, respectively. Under the assumption of near-circular chief orbit (i.e., $e_c \to 0$), these matrices are given by

$$A_{NC} = \begin{bmatrix} 0 & 0 & 0 & 0 & 0 & 0 \\ -\Lambda_c & 0 & 0 & 0 & -K_cF_cS_c & 0 \\ 0 & 0 & 0 & -K_cQ_c & 0 & 0 \\ 0 & 0 & K_cQ_c & 0 & 0 & 0 \\ 0 & 0 & 0 & 0 & 0 & 0 \\ \frac{7K_cS_c}{2} & 0 & 0 & 0 & 2K_cT_c & 0 \end{bmatrix} \quad B_{NC} = \frac{1}{n_c a_c}\begin{bmatrix} 0 & 2 & 0 \\ -2 & 0 & 0 \\ s_{u_c} & 2c_{u_c} & 0 \\ -c_{u_c} & 2s_{u_c} & 0 \\ 0 & 0 & s_{u_c} \\ 0 & 0 & c_{u_c} \end{bmatrix}, \tag{10}$$

where $u_c = \omega_c + M_c$ and the following substitutions are applied for clarity

$$F_c = 4 + 3\eta_c \quad E_c = 1 + \eta_c \quad S_c = \sin(2i_c) \quad T_c = \sin(i_c)^2 \quad \Lambda_c = \frac{3}{2}n_c + \frac{7}{2}E_c K_c P_c. \tag{11}$$

Analytical Solution for Near-circular Linear Dynamics Model

The solution of the linear system (9), $\delta\alpha(t)$, can be expressed as a function of the initial ROE state vector, $\delta\alpha(t_0)$, and the constant forcing vector, F, i.e. as

$$\delta\alpha(t) = \Phi(t, t_0)\delta\alpha(t_0) + \Psi(t, t_0)F \tag{12}$$

where $\Phi(t, t_0)$ and $\Psi(t, t_0)$ indicate the STM and the convolution matrix, respectively. As widely discussed in (Reference 6,11), Floquet theory can be exploited to derive the STM. The

STM associated with near-circular linear relative dynamics model is reported here for completeness

$$\boldsymbol{\Phi}_{NC}(t,t_0) = \begin{bmatrix} 1 & 0 & 0 & 0 & 0 & 0 \\ -\Lambda_c \Delta t & 1 & 0 & 0 & -K_c F_c S_c \Delta t & 0 \\ 0 & 0 & c_{\Delta\omega} & -s_{\Delta\omega} & 0 & 0 \\ 0 & 0 & s_{\Delta\omega} & c_{\Delta\omega} & 0 & 0 \\ 0 & 0 & 0 & 0 & 1 & 0 \\ \frac{7}{2} K_c S_c \Delta t & 0 & 0 & 0 & 2K_c T_c \Delta t & 1 \end{bmatrix} \tag{13}$$

where $\Delta t = t - t_0$ and $\Delta\omega = K_c Q_c \Delta t$. According to linear dynamics system theory[12], the convolution matrix, $\boldsymbol{\Psi}(t,t_0)$, can be computed by solving the following integral,

$$\boldsymbol{\Psi}_{NC}(t,t_0) = \int_{t_0}^{t} \boldsymbol{\Phi}_{NC}(t,\tau)\, \boldsymbol{B}_{NC}(\boldsymbol{\alpha}_c(\tau)) d\tau \tag{14}$$

Substituting the STM and the $\boldsymbol{B}_{NC}$ matrices reported in Eqs. (13) and (10), respectively, into Eq. (14) yields

$$\boldsymbol{\Psi}_{NC}(t,t_0) = \begin{bmatrix} 0 & \dfrac{2\Delta u}{n_c a_c W_c} & 0 \\[2ex] -\dfrac{2\Delta u}{n_c a_c W_c} & -\dfrac{\Lambda_c \Delta u^2}{n_c a_c W_c^2} & \dfrac{F_c K_c S_c \left(c_{u_{c,t}} - c_{u_{c,0}} + s_{u_{c,0}} \Delta u\right)}{n_c a_c W_c^2} \\[2ex] -\dfrac{c_{u_{c,t}} - c_{u_{c,0}+C\Delta u}}{n_c a_c (1-c) W_c} & 2\dfrac{s_{u_{c,t}} - s_{u_{c,0}+C\Delta u}}{n_c a_c (1-C) W_c} & 0 \\[2ex] -\dfrac{s_{u_{c,t}} - s_{u_{c,0}+C\Delta u}}{n_c a_c (1-C) W_c} & -2\dfrac{c_{u_{c,t}} - c_{u_{c,0}+C\Delta u}}{n_c a_c (1-C) W_c} & 0 \\[2ex] 0 & 0 & \dfrac{s_{u_{c,t}} - s_{u_{c,0}}}{n_c a_c W_c} \\[2ex] 0 & \dfrac{7}{2}\dfrac{K_c S_c \Delta u^2}{n_c a_c W_c^2} & \left(\begin{array}{c} -\dfrac{(W_c + 2K_c T_c)\left(c_{u_{c,t}} - c_{u_{c,0}}\right)}{n_c a_c W_c^2} \\[2ex] -\dfrac{2K_c T_c s_{u_{c,0}} \Delta u}{n_c a_c W_c^2} \end{array}\right) \end{bmatrix} \tag{15}$$

where $u_{c,t}$ and $u_{c,0}$ denote the mean argument of latitude of chief orbit at the instant t and t_0, respectively, and $\Delta u = u_{c,t} - u_{c,0}$. In Eq. (15) the terms C and W_c are constant coefficients that depend on the mean semi-major axis, eccentricity, and inclination of the chief orbit as follows

$$W_c = n_c + K_c Q_c + \eta_c K_c P_c, \quad C = \frac{K_c Q_c}{W_c}. \tag{16}$$

Note that the mean argument of the latitude can be written as a function of time using the relationships reported in Eq. (2), i.e., $u_{c,t} = u_{c,0} + W_c(t - t_0)$.

RECONFIGURATION CONTROL PROBLEM

This section presents the derivation of a control solution for the continuous thrust reconfiguration problem. Recall that the trajectory reconfiguration problem denotes the achievement of a certain user-defined set of ROE after a given time interval. Again, only the deputy is assumed to be maneuverable and capable of providing continuous on/off thrust along the x, y, and z directions of its own LVLH reference frame.

General Approach

Let us consider N continuous maneuvers of magnitude $f_{i,j}$ with $i = x, y, z$ and duration Δt_{bj}, with $j = 1, \dots N$, as illustrated in Figure 1. Using the near-circular linearized model discussed in the previous section, the relative state at the end of each j-th maneuvers $\delta\boldsymbol{\alpha}(t_{j,f})$ can be expressed as a function of $\delta\boldsymbol{\alpha}(t_{j,0})$, the maneuver durations Δt_{bj}, and thrust magnitudes as follows (see Eq.(12)),

$$\delta\boldsymbol{\alpha}_{j,f} = \delta\boldsymbol{\alpha}(t_{j,f}) = \boldsymbol{\Phi}(t_{j,f}, t_{j,0})\delta\boldsymbol{\alpha}(t_{j,0}) + \boldsymbol{\Psi}(t_{j,f}, t_{j,0})\boldsymbol{F}_j \quad j = 1, \dots, N \tag{17}$$

where $t_{j,0}$ and $t_{j,f}$ indicate the initial and the final times of the j-th maneuver respectively, and $\boldsymbol{F}_j = [f_{x,j}, f_{y,j}, f_{z,j}]^T$. The time $t_{j,f}$ can be expressed as a function of the maneuver duration Δt_{bj} as $t_{j,f} = t_{j,0} + \Delta t_{bj}$. According to Eq. (17), the mean ROE at the end of the maneuver, $\delta\boldsymbol{\alpha}(t_m)$, depend on the mean ROE at the initial maneuver time $\delta\boldsymbol{\alpha}(t_0)$, on the N maneuver durations, Δt_{bj}, and on the thrust vectors, $\boldsymbol{F}_j$,

$$\delta\boldsymbol{\alpha}_{1,0} = \delta\boldsymbol{\alpha}(t_{1,0}) = \boldsymbol{\Phi}(t_{1,0}, t_0)\delta\boldsymbol{\alpha}(t_0) = \boldsymbol{\Phi}(t_{1,0}, t_0)\delta\boldsymbol{\alpha}_0 \quad j = 1, \dots, N \tag{18}$$

$$\delta\boldsymbol{\alpha}_{1,f} = \boldsymbol{\Phi}(t_{1,f}, t_{1,0})\delta\boldsymbol{\alpha}_{1,0} + \boldsymbol{\Psi}(t_{1,f}, t_{1,0})\boldsymbol{F}_1 = \boldsymbol{\Phi}(t_{1,f}, t_0)\delta\boldsymbol{\alpha}_0 + \boldsymbol{\Psi}(t_{1,f}, t_{1,0})\boldsymbol{F}_1 \tag{19}$$

$$\delta\boldsymbol{\alpha}_{2,0} = \boldsymbol{\Phi}(t_{2,0}, t_{1,f})\delta\boldsymbol{\alpha}_{1,f} = \boldsymbol{\Phi}(t_{2,0}, t_0)\delta\boldsymbol{\alpha}_0 + \boldsymbol{\Phi}(t_{2,0}, t_{1,f})\boldsymbol{\Psi}(t_{1,f}, t_{1,0})\boldsymbol{F}_1 \tag{20}$$

$$\delta\boldsymbol{\alpha}_{2,f} = \boldsymbol{\Phi}(t_{2,f}, t_{2,0})\delta\boldsymbol{\alpha}_{2,0} + \boldsymbol{\Psi}(t_{2,f}, t_{2,0})\boldsymbol{F}_2 = \boldsymbol{\Phi}(t_{2,0}, t_0)\delta\boldsymbol{\alpha}_0 + \tag{21}$$
$$\boldsymbol{\Phi}(t_{2,f}, t_{1,f})\boldsymbol{\Psi}(t_{1,f}, t_{1,0})\boldsymbol{F}_1 + \boldsymbol{\Psi}(t_{2,f}, t_{2,0})\boldsymbol{F}_2$$

$$\vdots$$

$$\delta\boldsymbol{\alpha}_{t_m} = \boldsymbol{\Phi}(t_m, t_0)\delta\boldsymbol{\alpha}_0 + \Sigma\widehat{\boldsymbol{F}} \tag{22}$$

where

$$\Sigma\widehat{\boldsymbol{F}} = \begin{bmatrix} \boldsymbol{\Phi}(t_m, t_{1,f})\boldsymbol{\Psi}(t_{1,f}, t_{1,0}) & \dots & \boldsymbol{\Phi}(t_m, t_{N,f})\boldsymbol{\Psi}(t_{N,f}, t_{N,0}) \end{bmatrix} \begin{bmatrix} \boldsymbol{F}_1 \\ \vdots \\ \boldsymbol{F}_N \end{bmatrix} \tag{23}$$

If the values of Δt_{bj} and $\delta\boldsymbol{\alpha}_0$ are fixed, the only remaining unknowns for the reconfiguration are the thrust magnitudes, $f_{i,j}$, and their application times, $t_{j,0}$ (or alternatively the time of the middle point of the maneuver, i.e. $(t_{j,0} + t_{j,f})/2$), that satisfy the following equation

$$\Delta\delta\boldsymbol{\alpha}_{des} = \delta\boldsymbol{\alpha}_{des} - \boldsymbol{\Phi}(t_m, t_0)\delta\boldsymbol{\alpha}_0 = \Sigma\widehat{\boldsymbol{F}}. \tag{24}$$

The term $\delta\boldsymbol{\alpha}_{des}$ is the desired mean ROE vector at the end of the maneuver interval. Eq. (24) represents a set of 6 nonlinear equations in $2N$ unknowns. Accordingly, 3 burns are needed to obtain a finite number of analytical solutions. Note that the solution of reconfiguration problem, i.e. $f_{i,j}$ and $t_{j,0}$, is a function of $\delta\boldsymbol{\alpha}_0$, the burns' durations, and desired ROE state at the end of maneuver.
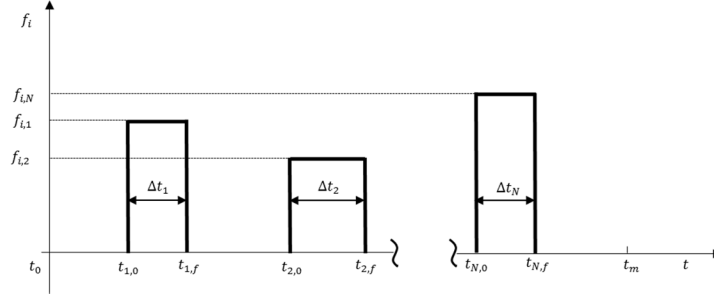
Figure 1. Continuous on/off control profile.

In (Reference 3) the authors derived the semi-analytical solutions for the in-plane and out-of plane reconfiguration problems in near-circular perturbed orbits using an impulsive maneuver scheme. This paper presents the analytical and semi-analytical solutions for the same class of problems using continuous thrust maneuvers. More specifically, the following reconfiguration problems are considered:

- *In-plane reconfiguration*:

$$S_1 = \{\Delta\delta\hat{\boldsymbol{\alpha}}_{des} = \left[\Delta\delta a_{des}, \Delta\delta\lambda_{des}, \Delta\delta e_{x,des}, \Delta\delta e_{y,des}\right]^T \subseteq \Delta\delta\boldsymbol{\alpha}_{des}\};$$

- *Out-of-plane reconfiguration*:

$$S_2 = \{\Delta\delta\hat{\boldsymbol{\alpha}}_{des} = \left[\Delta\delta i_{x,des}, \Delta\delta i_{y,des}\right]^T \subseteq \Delta\delta\boldsymbol{\alpha}_{des}\};$$

- *Full reconfiguration:*

$$S_3 = \left\{\Delta\delta\hat{\boldsymbol{\alpha}}_{des} = \left[\Delta\delta a_{des}, \Delta\delta\lambda_{des}, \Delta\delta e_{x,des}, \Delta\delta e_{y,des}, \Delta\delta i_{x,des}, \Delta\delta i_{y,des}\right]^T\right\}$$

The control solutions are obtained using the STM and convolution matrices associated with the near-circular dynamics model (see Eq. (13) and Eq.(15)).

In-plane Reconfiguration

In this section the in-plane reconfiguration problem is addressed. Let us consider that only three tangential maneuvers are applied on the deputy spacecraft, i.e.,

$$\hat{\boldsymbol{F}} = [\boldsymbol{F}_1^T, \boldsymbol{F}_2^T, \boldsymbol{F}_3^T] = \left[0, f_{y,1}, 0, 0, f_{y,2}, 0, 0, f_{y,3}, 0\right]^T. \tag{25}$$

This choice allows an analytical solution to be computed. Moreover, as discussed by Chernick *et al.* in (Reference 3), the use of three tangential impulses allows finding a minimum delta-V solution when the reconfiguration cost is driven by the variation of relative eccentricity vector. For this reason, the approach in this paper focuses on a similar tangential maneuvering scheme.

According to Eq. (23), the equations governing the evolution of the in-plane mean ROE are

$$\tilde{u}_{1,y}f_{y,1} + \tilde{u}_{2,y}f_{y,2} + \tilde{u}_{3,y}f_{y,3} = \frac{W_c n_c a_c}{4}\Delta\delta a_{des} \tag{26}$$

$$-\left(2\Lambda_c\left(u_{t_m} - \hat{u}_{1,y}\right)\tilde{u}_{1,y}\right)f_{y,1} - \left(2\Lambda_c\left(u_{t_m} - \hat{u}_{1,y}\right)\tilde{u}_{2,y}\right)f_{y,2} - \ldots$$
$$\ldots - \left(2\Lambda_c\left(u_{t_m} - \hat{u}_{3,y}\right)\tilde{u}_{3,y}\right)f_{y,3} = \frac{W_c^2 n_c a_c}{2}\Delta\delta\lambda_{des} \tag{27}$$

$$\left(\cos\left(Cu_{t_m} + (1-C)\hat{u}_{1,y}\right)\sin\left((1-C)\tilde{u}_{1,y}\right)\right)f_{y,1} + \ldots \tag{28}$$

8

$$\ldots + \left(\cos(Cu_{t_m} + (1-C)\hat{u}_{2,y})\sin\left((1-C)\tilde{u}_{2,y}\right)\right)f_{y,2} + \ldots$$
$$\left(\cos(Cu_{t_m} + (1-C)\hat{u}_{3,y})\sin((1-C)\tilde{u}_{3,y})\right)f_{y,3} = \frac{(1-C)W_c n_c a_c}{4}\Delta\delta e_{x,des}$$

$$\left(\sin(Cu_{t_m} + (1-C)\hat{u}_{1,y})\sin\left((1-C)\tilde{u}_{1,y}\right)\right)f_{y,1} + \ldots$$
$$\ldots + \left(\sin(Cu_{t_m} + (1-C)\hat{u}_{2,y})\sin\left((1-C)\tilde{u}_{2,y}\right)\right)f_{y,2} + \ldots \tag{29}$$
$$\ldots + \left(\sin(Cu_{t_m} + (1-C)\hat{u}_{3,y})\sin((1-C)\tilde{u}_{3,y})\right)f_{y,3} = \frac{(1-C)W_c n_c a_c}{4}\Delta\delta e_{y,des}$$

where

$$\hat{u}_{j,y} = \frac{u_{j,f} + u_{j,0}}{2} \quad \tilde{u}_{j,y} = \frac{u_{j,f} - u_{j,0}}{2} \quad j = 1, \ldots 3 \tag{30}$$

and $u_{j,0}$ and $u_{j,f}$ denote the chief mean argument of latitude at times $t_{j,0}$ and $t_{j,f}$, respectively. Defining the variables

$$\bar{U}_{j,0,y} = (1-C)u_{j,0,y} + Cu_{t_m} \quad \bar{U}_{j,f,y} = (1-C)u_{j,f,y} + Cu_{t_m} \quad j = 1, \ldots 3 \tag{31}$$

$$\widetilde{\bar{U}}_{j,y} = \frac{\bar{U}_{j,f,y} - \bar{U}_{j,0,y}}{2} = (1-C)\tilde{u}_{j,y} \quad \widehat{\bar{U}}_{j,y} = \frac{\bar{U}_{j,f,y} + \bar{U}_{j,0,y}}{2} = Cu_{t_m} + (1-C)\hat{u}_{j,y}$$

allows for rearranging Eqs. (26)-(30) into a more convenient form, given by

$$\widetilde{\bar{U}}_{1,y}f_{y,1} + \widetilde{\bar{U}}_{2,y}f_{y,2} + \widetilde{\bar{U}}_{3,y}f_{y,3} = \frac{(1-C)W_c n_c a_c}{4}\Delta\delta a_{des} \tag{32}$$

$$-\left(2\Lambda_c\left(u_{t_m} - \widehat{\bar{U}}_{1,y}\right)\widetilde{\bar{U}}_{1,y}\right)f_{y,1} - \left(2\Lambda_c\left(u_{t_m} - \widehat{\bar{U}}_{2,y}\right)\widetilde{\bar{U}}_{2,y}\right)f_{y,2} - \ldots$$
$$\ldots - \left(2\Lambda_c\left(u_{t_m} - \widehat{\bar{U}}_{3,y}\right)\widetilde{\bar{U}}_{3,y}\right)f_{y,3} = \frac{(1-C)^2 W_c^2 n_c a_c}{2}\Delta\delta\lambda_{des} \tag{33}$$

$$\left(\cos\left(\widehat{\bar{U}}_{1,y}\right)\sin(\widetilde{\bar{U}}_{1,y})\right)f_{y,1} + \left(\cos\left(\widehat{\bar{U}}_{2,y}\right)\sin(\widetilde{\bar{U}}_{2,y})\right)f_{y,2} + \ldots$$
$$\ldots + \left(\cos\left(\widehat{\bar{U}}_{3,y}\right)\sin(\widetilde{\bar{U}}_{3,y})\right)f_{y,3} = \frac{(1-C)W_c n_c a_c}{4}\Delta\delta e_{x,des} \tag{34}$$

$$\left(\sin\left(\widehat{\bar{U}}_{1,y}\right)\sin(\widetilde{\bar{U}}_{1,y})\right)f_{y,1} + \left(\sin\left(\widehat{\bar{U}}_{2,y}\right)\sin(\widetilde{\bar{U}}_{2,y})\right)f_{y,2} + \ldots$$
$$\ldots + \left(\sin\left(\widehat{\bar{U}}_{3,y}\right)\sin(\widetilde{\bar{U}}_{3,y})\right)f_{y,3} = \frac{(1-C)W_c n_c a_c}{4}\Delta\delta e_{y,des} \tag{35}$$

It is worth noting that Eqs. (32)-(35) match the expressions obtained for three tangential impulses maneuver in (Reference 3). Accordingly, the solution of the above system will have the same structure. In light of this, the locations (expressed as mean argument of latitude) of the maneuver middle points, $\hat{u}_{j,y}$, are given by

$$\hat{u}_{j,y} = \frac{\widehat{\bar{U}}_{j,y}}{1-C} - \frac{Cu_{t_m}}{1-C} \quad \widehat{\bar{U}}_{j,y} = \text{atan}\left(\frac{\Delta\delta e_{y,des}}{\Delta\delta e_{x,des}}\right) + k_j\pi \quad j = 1, \ldots 3 \tag{36}$$

where k_j must be an integer. The thrust magnitudes are

$$f_{y,j} = -\frac{\left\{(-1)^{k_1}(1-C)W_c a_c n_c \Xi_j\right\}}{D}. \tag{37}$$

where the quantities Ξ_j and D are detailed in Appendix B.

Out-of-plane Reconfiguration

In this section the out-of-plane control solution is presented. In order to achieve the desired x and y components of the relative inclination vector at the end of the maneuver, the control solution must include a component in the cross-track (z) direction. In fact, the only way to modify the difference in chief and deputy orbit inclination (i.e., δi_x) is to provide a control action along the z-axis of deputy LVLH frame. This is immediately evident from inspection of the linearized equations of relative motion (see Eq. (10)). More specifically, if a single cross-track maneuver is performed by the deputy satellite, i.e. $\boldsymbol{F}_1 = [0,0,f_{z,1}]^T$, the equations governing the change of inclination vector are (see Eq. (23))

$$\cos(\hat{u}_{1,z})\sin(\tilde{u}_{1,z})f_{z,1} = \frac{W_c n_c a_c}{2}\Delta\delta i_{x,des} \tag{38}$$

$$\left(\begin{array}{c} 2K_cT_c(u_{t_m} - \hat{u}_{1,z} - \tilde{u}_{1,z})\cos(\hat{u}_{1,z})\sin(\tilde{u}_{1,z}) + \\ (W_c + 2K_cT_c)\sin(\hat{u}_{1,z})\sin(\tilde{u}_{1,z}) \\ -2K_cT_c\sin(\hat{u}_{1,z} - \tilde{u}_{1,z})\tilde{u}_{1,z} \end{array} \right)f_{z,1} = \frac{W_c^2 n_c a_c}{2}\Delta\delta i_{y,des} \tag{39}$$

The magnitude of the maneuver can be computed by inverting Eq. (38),

$$f_{z,1} = \frac{W_c n_c a_c}{2[\cos(\hat{u}_{1,z})\sin(\tilde{u}_{1,z})]}\Delta\delta i_{x,des} \tag{40}$$

The location of the maneuver, $\hat{u}_{1,z}$, can be found by substituting Eq. (40) into Eq. (39) to obtain the following transcendental expression,

$$\left(\begin{array}{c} 2K_cT_c(u_{t_m} - \hat{u}_{1,z} - \tilde{u}_{1,z}) + (W_c + 2K_cT_c)\,\text{tg}(\hat{u}_{1,z}) \\ -\dfrac{2K_cT_c\sin(\hat{u}_{1,z} - \tilde{u}_{1,z})\tilde{u}_{1,z}}{\cos(\hat{u}_{1,z})\sin(\tilde{u}_{1,z})} \end{array} \right) = W_c\frac{\Delta\delta i_{y,des}}{\Delta\delta i_{x,des}}. \tag{41}$$

Eq. (41) can be numerically solved by using an iterative algorithm. The single out-of-plane maneuver solution for unperturbed orbits provides useful insight into choosing a good initial guess for quick convergence of the iterative approach. In this case, the location given by $\hat{u}_{1,z} = \text{atan}(\Delta\delta i_{y,des}/\Delta\delta i_{x,des})$ is used.

Full Reconfiguration

In this section the solution of the full reconfiguration problem is presented. It is assumed that no radial maneuvers are performed and that only a single maneuver is performed for the control of the mean relative inclination vector, i.e.,

$$\widehat{\boldsymbol{F}} = [\boldsymbol{F}_1^T, \boldsymbol{F}_2^T, \boldsymbol{F}_3^T, \boldsymbol{F}_4^T] = [0, f_{y,1}, 0, 0, f_{y,2}, 0, 0, f_{y,3}, 0, 0, 0, f_{z,1}]^T. \tag{42}$$

Then, the following set of six equations must be solved with respect to the unknowns magnitudes and locations, $f_{y,j}$, $f_{z,1}$ $\hat{u}_{j,y}$ and $\hat{u}_{1,z}$ ($j = 1, \dots 3$), respectively

$$\tilde{u}_{1,y}f_{y,1} + \tilde{u}_{2,y}f_{y,2} + \tilde{u}_{3,y}f_{y,3} = \frac{W_c n_c a_c}{4}\Delta\delta a_{des} \tag{43}$$

$$\begin{array}{c} -\left(2\Lambda_c(u_{t_m} - \hat{u}_{1,y})\tilde{u}_{1,y}\right)f_{y,1} - \left(2\Lambda_c(u_{t_m} - \hat{u}_{1,y})\tilde{u}_{2,y}\right)f_{y,2} - \dots \\ \dots - \left(2\Lambda_c(u_{t_m} - \hat{u}_{3,y})\tilde{u}_{3,y}\right)f_{y,3} + \dots \\ \dots + F_cK_cS_c\left(\begin{array}{c} -\sin(\hat{u}_{1,z})\sin(\tilde{u}_{1,z}) + \sin(\hat{u}_{1,z} - \tilde{u}_{1,z})\tilde{u}_{1,z} + \dots \\ \dots + (u_{t_m} - \hat{u}_{1,z} - \tilde{u}_{1,z})\cos(\hat{u}_{1,z})\sin(\tilde{u}_{1,z}) \end{array} \right)f_{z,1} = \frac{W_c^2 n_c a_c}{2}\Delta\delta\lambda_{des} \end{array} \tag{44}$$

$$\left(\cos\left(Cu_{t_m} + (1-C)\hat{u}_{1,y}\right)\sin\left((1-C)\tilde{u}_{1,y}\right)\right)f_{y,1}+\dots$$
$$\dots + \left(\cos\left(Cu_{t_m} + (1-C)\hat{u}_{2,y}\right)\sin\left((1-C)\tilde{u}_{2,y}\right)\right)f_{y,2}+\dots \tag{45}$$
$$\dots + \left(\cos\left(Cu_{t_m} + (1-C)\hat{u}_{3,y}\right)\sin((1-C)\tilde{u}_{3,y})\right)f_{y,3} = \frac{(1-C)W_c n_c a_c}{4}\Delta\delta e_{x,des}$$

$$\left(\sin\left(Cu_{t_m} + (1-C)\hat{u}_{1,y}\right)\sin\left((1-C)\tilde{u}_{1,y}\right)\right)f_{y,1}+\dots$$
$$\dots + \left(\sin\left(Cu_{t_m} + (1-C)\hat{u}_{2,y}\right)\sin\left((1-C)\tilde{u}_{2,y}\right)\right)f_{y,2}+\dots \tag{46}$$
$$\dots + \left(\sin\left(Cu_{t_m} + (1-C)\hat{u}_{3,y}\right)\sin((1-C)\tilde{u}_{3,y})\right)f_{y,3} = \frac{(1-C)W_c n_c a_c}{4}\Delta\delta e_{y,des}$$

$$\cos\left(\hat{u}_{1,z}\right)\sin\left(\tilde{u}_{1,z}\right)f_{z,1} = \frac{W_c n_c a_c}{2}\Delta\delta i_{x,des} \tag{47}$$

$$\left(7K_c S_c\left(u_{t_m} - \hat{u}_{1,y}\right)\tilde{u}_{1,y}\right)f_{y,1} + \left(7K_c S_c\left(u_{t_m} - \hat{u}_{2,y}\right)\tilde{u}_{2,y}\right)f_{y,2}+\dots$$
$$\dots + \left(7K_c S_c\left(u_{t_m} - \hat{u}_{3,y}\right)\tilde{u}_{3,y}\right)f_{y,3}+\dots$$
$$\dots + \begin{pmatrix} 2K_c T_c\left(u_{t_m} - \hat{u}_{1,z} - \tilde{u}_{1,z}\right)\cos\left(\hat{u}_{1,z}\right)\sin\left(\tilde{u}_{1,z}\right) +\dots \\ \dots + (W_c + 2K_c T_c)\sin\left(\hat{u}_{1,z}\right)\sin\left(\tilde{u}_{1,z}\right) +\dots \\ \dots - 2K_c T_c \sin\left(\hat{u}_{1,z} - \tilde{u}_{1,z}\right)\tilde{u}_{1,z} \end{pmatrix} f_{z,1} = \frac{W_c^2 n_c a_c}{2}\Delta\delta i_{y,des} \tag{48}$$

The system (43)-(48) can be solved numerically through an iterative algorithm. The solution results are presented in the following section. The use of analytical and semi-analytical solutions, obtained for in-plane and out-of-plane maneuvers, as initial guess (see Eqs. (36)-(37) and Eqs. (40)-(41)), guarantees the algorithm's convergence in less than four iterations.

NUMERICAL VALIDATION OF THE CONTROL SOLUTIONS

In this section the relative trajectories obtained using the developed control solutions are presented, pointing out their performances in terms of maneuver cost and accuracy. Figure 2 illustrates the simulation setup exploited for the validation of the proposed maneuvering solutions.
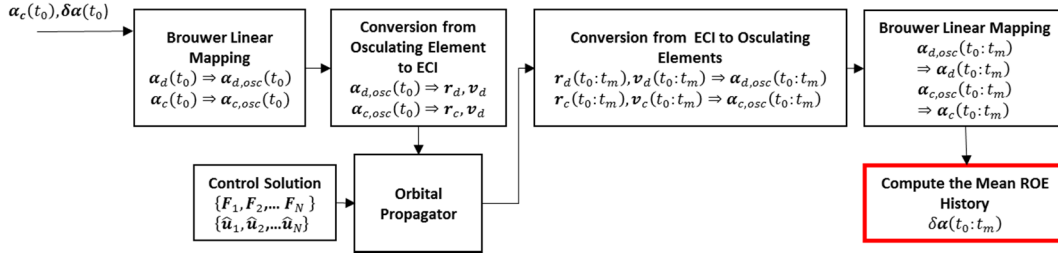

Figure 2. Numerical validation scheme.

First, the initial mean orbit elements of the chief and the mean ROE state are set. Then, the initial mean orbit elements of the deputy are computed using the identities in Eq. (8). A numerical propagator including the Earth's oblateness J_2 effects is used to obtain the history of position and velocity of chief and deputy spacecraft expressed in Earth Centered Inertial (ECI) reference frame (J2000). The initial Cartesian state of both satellites are derived using the linear mapping developed by Brouwer and Lyddane to transform the mean orbit elements into osculating and the non-linear relations between Cartesian state and osculating elements[13,14,15]. The control thrust profile is projected into the ECI frame and added as external accelerations to the deputy's motion. After the

simulation, the absolute position and velocity of the spacecraft are converted into the mean orbit elements to compute the accuracy at the end of the maneuver, defined as

$$\varepsilon_{\delta\alpha_k} = \left|\delta\alpha_k^{num}(t_m) - \delta\alpha_{k,des}\right|a_c(t_0) \quad k = 1, \dots, 6. \tag{49}$$

Ultimately, a numerical optimizer is used to verify the efficiency of the proposed analytical solutions. It is worth noting that the optimizer is only employed to check the degree to which the analytical solution can be improved using the maneuver scheme given in Eq. (42). Hence, a detailed study of the optimality of the solution as a function of the number of maneuvers is not carried out in the frame of this work. More specifically, the Matlab built-in *MultiStart* routine is exploited to find the values of $f_{i,j}$, $\tilde{u}_{j,i}$ and $\hat{u}_{j,i}$ with $i = y, z$ that minimize the maneuver cost in term of $\Delta V = \sum_{j=1}^{N} 2f_{y,j}\tilde{u}_{j,y}/W_c + 2f_{z,j}\tilde{u}_{j,z}/W_c$, satisfying the following constraints

$$\Delta\delta\boldsymbol{\alpha}_{des} - \boldsymbol{\Sigma}\widehat{\boldsymbol{F}} < 1e - 8 \tag{50}$$
$$\left|f_{i,j}\right| < f_{max}, \quad \hat{u}_{j+1,y} > \hat{u}_{j,y}, \quad \left|\tilde{u}_{j+1,y} + \tilde{u}_{j,y}\right| < \left|\hat{u}_{j+1,y} - \hat{u}_{j,y}\right|.$$

In the ensuing sections, we refer to the solution given by the *Multistart* optimizer as the numerical solution. In order to verify the effectiveness of the designed continuous thrust maneuvers three test cases are carried out, one for each reconfiguration problem defined in the previous sections. Moreover, a comparison with the corresponding impulsive control scheme reported in (Reference 3) is presented for in-plane and out-of-plane reconfiguration problems.

In-plane Reconfiguration Control Problem

This section presents the trajectories obtained using the analytical control solution reported in Eq. (36)-(37) and the numerical solution. The initial conditions used in the simulations are listed in Table 1 and Table 2 (see first row), along with the desired mean ROE vector at the end of the maneuver sequence. Note that the values of $\delta\boldsymbol{\alpha}_0$ and $\delta\boldsymbol{\alpha}_{des}$ lead to $a_c\Delta\delta\widehat{\boldsymbol{\alpha}}_{des} = a_c[\Delta\delta a_{des}, \Delta\delta\lambda_{des}, \Delta\delta e_{x,des}, \Delta\delta e_{y,des}]^T = [-0.03, 1.9172, 0.0403, 0.1198]^T$ km.

Table 1. Initial mean chef orbit.

a_c (km)	e_c (dim)	i_c (deg)	ω_c (deg)	Ω_c (deg)	f_c (deg)
6578	0	8	0	0	0

Table 2. Relative orbit at the initial and final maneuver time.

	$a_c\delta a$ (m)	$a_c\delta\lambda$ (m)	$a_c\delta e_x$ (m)	$a_c\delta e_y$ (m)	$a_c\delta i_x$ (m)	$a_c\delta i_y$ (m)
Initial relative orbit, $\delta\boldsymbol{\alpha}_0$	30	-11e3	0	-50	0	0
Desired relative orbit, $\delta\boldsymbol{\alpha}_{des}$	0	-10.5e3	45	70	0	0

The maneuver lasts 5 orbits, i.e. $u_f = 10\pi$. The analytical solution was obtained using the values of the maneuver intervals, Δt_{bj} with $j = 1, \dots 3$, and locations, $\widehat{\overline{U}}_{j,y}$, listed in Table 3. The same table shows the maneuver cost corresponding to the numerical in-plane solution. In addition, a comparison of the continuous control solutions developed in this paper and the corresponding impulsive control scheme reported in (Reference 3) is presented (see last row of Table 3). It is worth noting that the numerical continuous thrust solution requires a lower total delta-V than the analytical method by reducing the maneuver intervals and increasing the thrust magnitude (see also Figure 4). Moreover, the numerical solution offers the same performance as the corresponding analytical impulsive control solution. On the contrary, the analytical continuous

solution requires a higher delta-V than the impulsive scheme to achieve the desired formation configuration. This is to be expected due to the generally lower kinematic efficiency of continuous thrust maneuvering as compared with impulsive maneuvering.

Table 3. Comparison between the analytical and numerical control solution for the in-plane maneuver.

|	Maneuver Location, $\widehat{\widehat{U}}_{j,y}$ (rad)	Δv_1 (km/s) / Δt_{b1} (min)	Δv_2 (km/s) / Δt_{b2} (min)	Δv_3 (km/s) / Δt_{b3} (min)	**TOT (km/s)**
Analytical Continuous Solution	[1.245,4.38,20.09]	0.096e-4 / 5.5	-0.466e-4 / 7.34	0.192e-4 / 7.34	7.5595e-5
Numerical Continuous Solution	[4.37,20.088,23.32]	-0.369e-4 / 1.42	0.285e-4 / 1.80	-0.093e-4 / 0.36	7.486e-5
Analytical Impulsive Solution	[1.245,4.38,20.09]	0.092e-4 / instantaneous impulse	-0.463e-4 / instantaneous impulse	0.194e-4 / instantaneous impulse	7.48e-5

(a) (b)
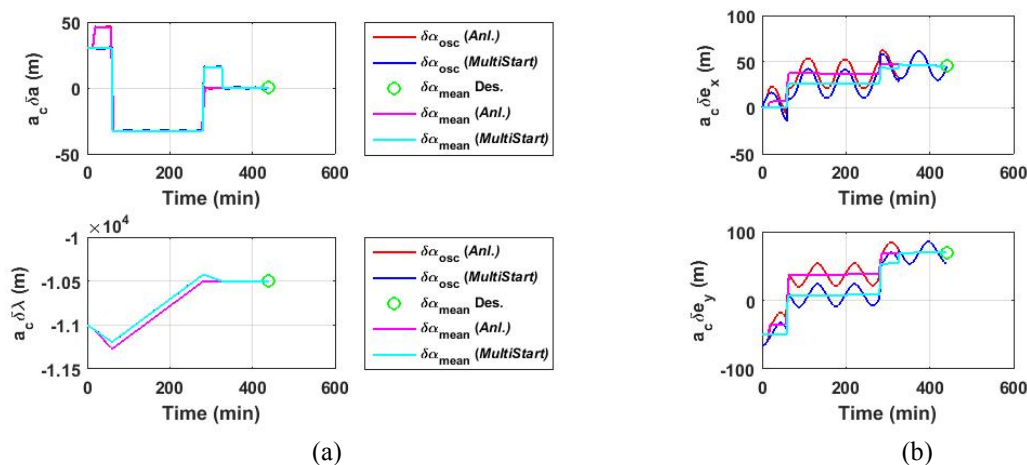
Figure 3. In-plane maneuver: (a) relative mean semi-major axis and longitude; (b) x- and y-component of mean relative eccentricity vector.

Figure 3 illustrates the mean ROE over the maneuvering time. Both osculating and mean ROE are shown in the same plot. From this figure, both proposed continuous control solutions guarantee that the desired in-plane conditions are met after the given interval of 5 orbits. Figure 4 illustrates the thrust profile corresponding to the analytical and numerical solutions. It is worth remarking that the numerical solution is computed assuming a value of maximum thrust of $5e-7$ km/s^2.
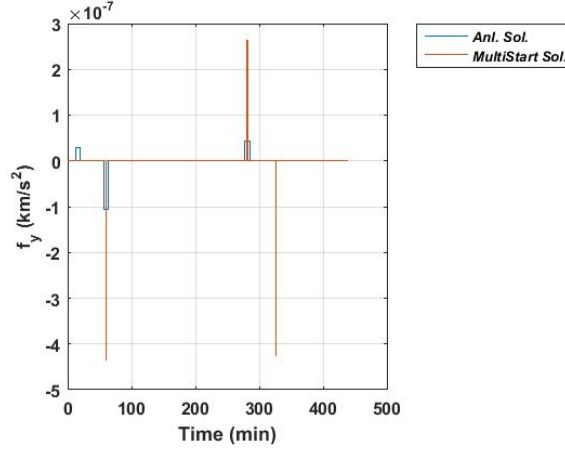
Figure 4. Control profile for in-plane maneuver.

Table 4 shows the accuracy for the proposed in-plane reconfiguration maneuvers, i.e. the difference between the mean ROE at the end of the maneuver, t_m, as computed by the numerical propagator and the desired ROE multiplied by the chief mean-semi-major axis (see Eq. (49)). The final error is at the meter level and is mainly due to the approximations introduced by the osculating-to-mean transformation at the end of the simulations.

Table 4. Accuracy of control solutions for in-plane maneuver.

	$\varepsilon_{\delta a}$ (m)	$\varepsilon_{\delta \lambda}$ (m)	$\varepsilon_{\delta e_x}$ (m)	$\varepsilon_{\delta e_y}$ (m)
Analytical Continuous Solution	0.045	2.192	0.197	0.035
Numerical Continuous Solution	0.045	2.193	0.189	0.036

Out-of-plane Reconfiguration Control Problem

Here, the relative motion obtained solving the Eqs. (40)-(41) is shown. In this out-of-plane reconfiguration scenario, a maneuver lasting 7 orbits is considered. The initial and desired states listed in Table 5 and Table 6 are used to run the verification simulations. The values of $\delta \boldsymbol{\alpha}_0$ and $\delta \boldsymbol{\alpha}_{des}$ yield the following change of ROE

$$a_c \Delta \delta \hat{\boldsymbol{\alpha}}_{des} = a_c \left[\Delta \delta i_{x,des}, \Delta \delta i_{y,des} \right]^T = [0.3950, 0.0497]^T (km). \tag{51}$$

It is worth remarking that the expression (41) is solved using the Matlab built-in routine *"fzero"*. Table 7 shows the duration and the location of the out-of-plane maneuver exploited to compute the semi-analytical solution as well as the same parameters obtained through the optimizing algorithm. In addition, Table 7 lists the delta-V for the continuous solutions derived within this study and the semi-analytical impulsive solution computed in (Reference 3).

Table 5. Initial mean chief orbit.

a_c (km)	e_c (dim)	i_c (deg)	ω_c (deg)	Ω_c (deg)	f_c (deg)
6828	0	78	0	0	0

14

Table 6. Relative orbit at the initial and final maneuver time.

	$a_c\delta i_x$ (m)	$a_c\delta i_y$ (m)
Initial relative orbit, $\delta\boldsymbol{\alpha}_0$	5	70
Desired relative orbit, $\delta\boldsymbol{\alpha}_{des}$	400	120

Table 7. Comparison between the semi-analytical and numerical control solutions for the out-of-plane maneuver.

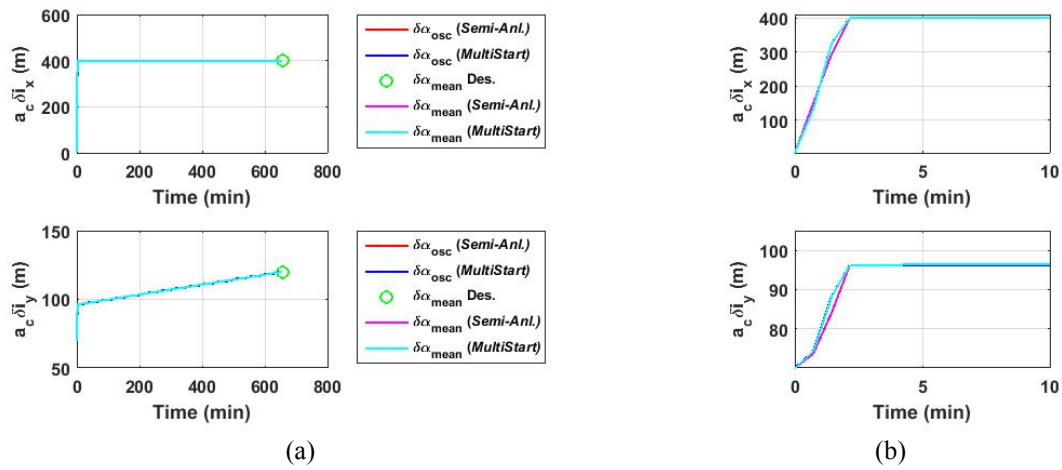|	Maneuver Location, $\hat{u}_{1,z}$ (rad)	Δv_1 (km/s) / Δt_{b1} (min)	TOT (km/s)
Semi-analytical Continuous Solution	0.0661	4.4329e-04/ 1.97	4.4329e-04
Numerical Continuous Solution	0.0661	4.4315e-04 / 1.47	4.4315e-04
Semi-analytical Impulsive Solution	0.1275	4.4373e-04 / instantaneous impulse	4.4373e-04

Figure 5. Out-of-plane maneuver: x- and y-components of the mean relative inclination vector (a) and zoomed-in view (b).
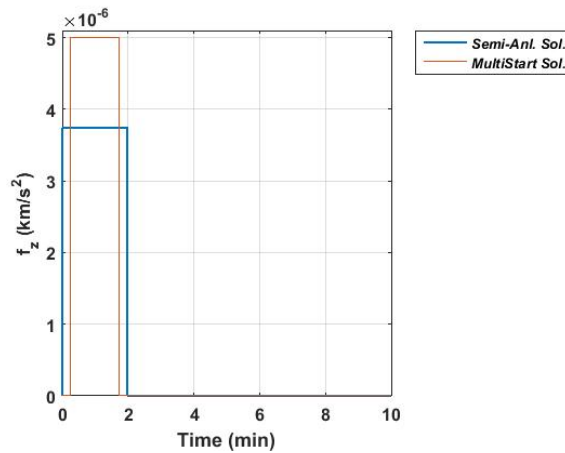

Figure 6. Control profile for out-of-plane maneuver (zoomed view).

Figure 5 shows the change of mean relative vector over the maneuver interval, whereas Figure 6 illustrates the z component of the control thrust vector obtained by the semi-analytical solution and by the numerical approach. Note that both solutions provide a single maneuver located at the beginning of the maneuver interval. In addition, the numerical solution achieves the maximum allowed thrust, i.e. $f_{max} = 5e - 6$ km/s². Finally, Table 8 reports the accuracy for the designed out-of-plane maneuver.

Table 8. Accuracy of the control solutions for the out-of-plane maneuver.

	$\varepsilon_{\delta i_x}$ (m)	$\varepsilon_{\delta i_y}$ (m)
Semi-analytical Continuous Solution	0.3554	0.0105
Numerical Continuous Solution	0.3555	0.0106

Full Reconfiguration Control Problem

In this section the full reconfiguration maneuver is shown. Table 9 and Table 10 report the initial and desired mean ROE respectively. In this scenario, a simple analytical solution is not provided. Consequently, the Matlab built-in routine *"fsolve"* is used to get the solution, assuming the burns' durations and locations reported in Table 11. As evidenced by the results summarized in Table 11, the numerical approach to solve the studied reconfiguration problem provides the same delta-V of the solution obtained with the numerical optimizer *MultiStart*, even though the burns' locations and durations are slightly different.

Table 9. Initial mean chief orbit.

a_c (km)	e_c (dim)	i_c (deg)	ω_c (deg)	Ω_c (deg)	f_c (deg)
6578	0	20	0	0	0

Table 10. Relative orbit at the initial and final maneuver time.

	$a_c\delta a$ (m)	$a_c\delta\lambda$ (m)	$a_c\delta e_x$ (m)	$a_c\delta e_y$ (m)	$a_c\delta i_x$ (m)	$a_c\delta i_y$ (m)
Initial relative orbit, $\delta\boldsymbol{\alpha}_0$	30	-11e3	0	-0	5	70
Desired relative orbit, $\delta\boldsymbol{\alpha}_{des}$	0	-10.5e3	45	70	400	120

Table 11. Comparison between the two numerical control solutions for out-of-plane maneuver.

	Maneuver Location, $\hat{u}_{j,y}$ (rad)	Maneuver Location, $\hat{u}_{1,z}$ (rad)	$\Delta v_{1,y}$ (km/s) / $\Delta t_{b1,y}$ (min)	$\Delta v_{2,y}$ (km/s) / $\Delta t_{b2,y}$ (min)	$\Delta v_{3,y}$ (km/s) / $\Delta t_{b3,y}$ (min)	$\Delta v_{1,z}$ (km/s) / $\Delta t_{b1,z}$ (min)	**TOT (km/s)**
fsolve **Continuous Solution**	[1.14,4.29,20.04]	0.119	0.0829e-4 / 5.509	-0.4654e-4 / 7.34	0.204e-4 / 7.34	4.708e-4 / 0.8	5.462e-4
Multistart **Continuous Solution**	[1.15,4.29,20.036]	0.119	0.0809e-4 / 4.33	-0.463e-4 / 4.07	0.205e-4 / 5.47	4.710e-4 / 1.57	5.459e-4

Figure 7 and Figure 8 illustrate the variation of the mean and osculating ROE over the maneuver time, whereas Figure 9 shows the component x and z of the control thrust vector given by the two employed numerical approaches.
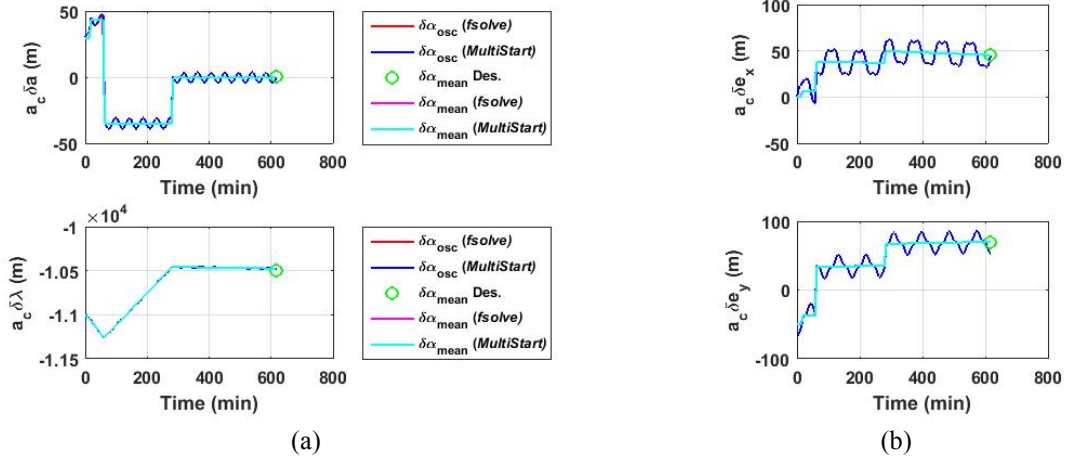
Figure 7. Full maneuver: (a) relative mean semi-major axis and longitude; (b) semi x- and y-component of mean relative eccentricity vector.
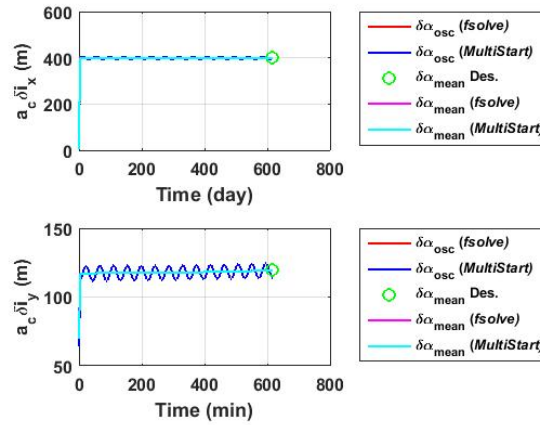

Figure 8. Full maneuver: semi x- and y-component of mean relative inclination vector.
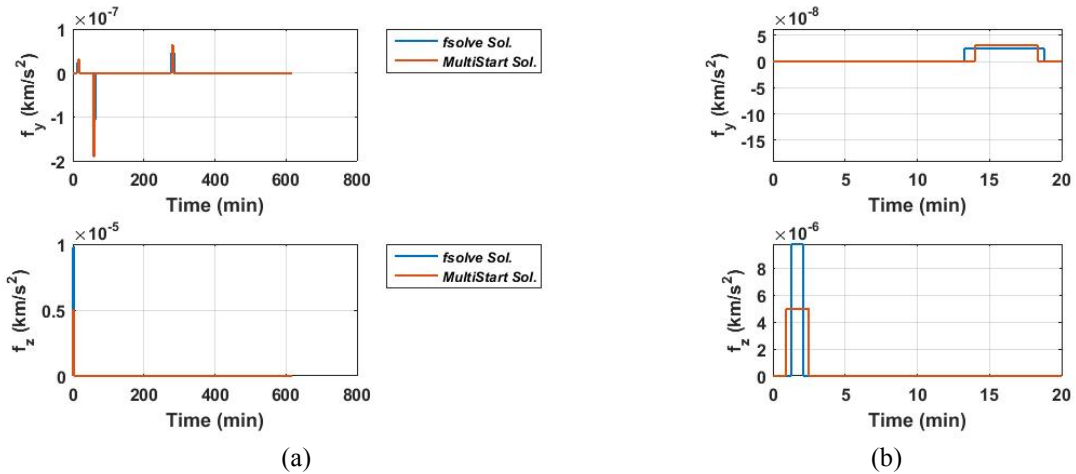

Figure 9. Control profile for out-of-plane maneuver (a) and zoomed-in view (b).

Finally, Table 12 summarizes the accuracy of the designed maneuver. Here it is shown that the proposed maneuver scheme controls the mean relative longitude with comparatively coarse accuracy ($\varepsilon_{\delta\lambda} = 24\,m$). However, the errors on the other components of final ROE vector remain small (at the centimeter level).

Table 12. Accuracy of control solutions for out-of-plane maneuver.

	$\varepsilon_{\delta a}$ (m)	$\varepsilon_{\delta\lambda}$ (m)	$\varepsilon_{\delta e_x}$ (m)	$\varepsilon_{\delta e_y}$ (m)	$\varepsilon_{\delta i_x}$ (m)	$\varepsilon_{\delta i_y}$ (m)
fsolve **Continuous Solution**	0.348	24.31	0.4367	0.0722	0.656	0.766
Multistart **Continuous Solution**	0.348	24.305	0.4366	0.0721	0.656	0.766

CONCLUSION

This paper addressed the computation of control solutions for spacecraft formation reconfiguration problems using continuous on/off maneuvers. A fully analytical solution for in-plane reconfiguration maneuvers was derived by inverting the relative orbit element-based linearized equations of relative motion and considering three tangential maneuvers. A semi-analytical approach was proposed for out-of-plane relative motion maneuvering with a single maneuver. Ultimately, a solution for the full reconfiguration control problem was numerically computed taking advantages of the results obtained for the in-plane and out-of-plane problems. Numerical simulations showed the performances in terms of maneuver cost and accuracy. The derived analytical and semi-analytical solutions for in-plane and out-of-plane maneuvers guarantee accuracy at the meter level, requiring slightly higher total delta-V than the corresponding numerical solutions computed through an optimization routine. However, unlike the numerical solutions, such (semi-) analytical solutions can be implemented onboard spacecraft with limited computing capabilities.

Future work on the topic will include a thorough optimality assessment of the (semi-) analytical control solutions derived in this work, as well as the extension of the continuous solutions to orbits of arbitrary eccentricity.

ACKNOWLEDGMENTS

APPENDIX A: CONTROL INFLUENCE MATRIX $\boldsymbol{\Gamma}$

The elements of control influence matrix $\boldsymbol{\Gamma}_F$ (see Eqs. (6)) are

$$\gamma_{13} = \gamma_{41} = \gamma_{51} = \gamma_{52} = \gamma_{62} = 0$$

$$\gamma_{11} = \frac{2e_d s_{f_d}}{n_d \eta_d a_c} \quad \gamma_{12} = \frac{2(1 + e_d c_{f_d})}{n_d \eta_d a_c} \quad \gamma_{21} = -\frac{\eta_d e_d c_{f_d}}{a_d n_d (1 + \eta_d)} - \frac{2\eta_d^2}{a_d n_d (1 + e_d c_{f_d})}$$

$$\gamma_{22} = -\frac{\eta_d e_d [(2 + e_d c_{f_d}) s_{f_d}]}{a_d n_d (1 + \eta_d)(1 + e_d c_{f_d})} \quad \gamma_{23} = -\frac{\eta s_{\theta_d} (c_{i_c} - c_{i_d})}{a_d n_d (1 + e_d c_{f_d}) s_i} \tag{52}$$

$$\gamma_{31} = \frac{\eta_d s_{\theta_d}}{a_d n_d} \quad \gamma_{32} = \frac{\eta_d (2 + e_d c_{f_d}) c_{\theta_d} + \eta_d e_{x,d}}{a_d n_d (1 + e_d c_{f_d})} \quad \gamma_{33} = \frac{\eta_d e_{y,d} s_{\theta_d} cotg(i_d)}{a_d n_d (1 + e_d c_{f_d})}$$

$$\gamma_{41} = -\frac{\eta_d c_{\theta_d}}{a_d n_d}, \quad \gamma_{42} = \frac{\eta_d(2 + e_d c_{f_d})s_{\theta_d} + \eta_d e_{y,d}}{a_d n_d(1 + e_d c_{f_d})}$$

$$\gamma_{43} = -\frac{\eta_d e_{x,d} s_{\theta_d} cotg(i_d)}{a_d n_d(1 + e_d c_{f_d})} \quad \gamma_{53} = \frac{\eta_d s_{\theta_d}}{a_d n_d(1 + e_d c_{f_d})} \quad \gamma_{63} = \frac{\eta_d c_{\theta_d} s_{i_c}}{a_d n_d(1 + e_d c_{f_d})s_{i_d}}$$

where f_d and θ_d represent the deputy satellite's true anomaly and true argument of latitude respectively.

APPENDIX B: IN-PLANE RECONFIGURATION

This appendix details the quantities Ξ_j with $j = 1, \ldots 3$ and D needed to compute the analytical solution for the in-plane reconfiguration (see Eq. (37)).

$$\Xi_1 = \begin{pmatrix} (-1)^{k_1}(-1)^{k_2}\Lambda_c\widetilde{\overline{U}}_{3,y}\sin(\widetilde{\overline{U}}_{2,y})\left(u_{t_m} - \overline{U} - k_1\pi - k_3\pi\right)\Delta\delta a_{des} - \ldots \\ \ldots - (-1)^{k_1}(-1)^{k_3}\Lambda_c\widetilde{\overline{U}}_{2,y}\sin(\widetilde{\overline{U}}_{3,y})\left(u_{t_m} - \overline{U} - k_1\pi - k_2\pi\right)\Delta\delta a_{des} - \ldots \\ \ldots - \pi\Lambda_c\Theta(k_2 - k_3)\widetilde{\overline{U}}_{2,y}\widetilde{\overline{U}}_{3,y}\Delta\delta e_{x,des} + \ldots \\ \ldots + (-1)^{k_1}(-1)^{k_2}(1 - C)W_c\widetilde{\overline{U}}_{3,y}\sin(\widetilde{\overline{U}}_{2,y})\Delta\lambda_{des} - \ldots \\ \ldots - (-1)^{k_1}(-1)^{k_3}(1 - C)W_c\widetilde{\overline{U}}_{2,y}\sin(\widetilde{\overline{U}}_{3,y})\Delta\lambda_{des} \end{pmatrix} \tag{53}$$

$$\Xi_2 = \begin{pmatrix} (-1)^{k_1}\Lambda_c\widetilde{\overline{U}}_{3,y}\sin(\widetilde{\overline{U}}_{1,y})\left(u_{t_m} - \overline{U} - k_1\pi - k_3\pi\right)\Delta\delta a_{des} - \ldots \\ \ldots - (-1)^{k_1}(-1)^{k_3}\Lambda_c\widetilde{\overline{U}}_{1,y}\sin(\widetilde{\overline{U}}_{3,y})\left(u_{t_m} - \overline{U} - k_1\pi\right)\Delta\delta a_{des} + \ldots \\ \ldots + \pi\Lambda_c\Theta(k_3)\widetilde{\overline{U}}_{1,y}\widetilde{\overline{U}}_{3,y}\Delta\delta e_{x,des} + (-1)^{k_1}(1 - C)W_c\widetilde{\overline{U}}_{3,y}\sin(\widetilde{\overline{U}}_{1,y})\Delta\lambda_{des} - \ldots \\ \ldots - (-1)^{k_1}(-1)^{k_3}(1 - C)W_c\widetilde{\overline{U}}_{1,y}\sin(\widetilde{\overline{U}}_{3,y})\Delta\lambda_{des} \end{pmatrix} \tag{54}$$

$$\Xi_3 = \begin{pmatrix} (-1)^{k_1}\Lambda_c\widetilde{\overline{U}}_{2,y}\sin(\widetilde{\overline{U}}_{1,y})\left(u_{t_m} - \overline{U} - k_1\pi - k_2\pi\right)\Delta\delta a_{des} - \ldots \\ \ldots - (-1)^{k_1}(-1)^{k_2}\Lambda_c\widetilde{\overline{U}}_{1,y}\sin(\widetilde{\overline{U}}_{2,y})\left(u_{t_m} - \overline{U} - k_1\pi\right)\Delta\delta a_{des} + \ldots \\ \ldots + \pi\Lambda_c\Theta(k_2)\widetilde{\overline{U}}_{1,y}\widetilde{\overline{U}}_{2,y}\Delta\delta e_{x,des} + (-1)^{k_1}(1 - C)W_c\widetilde{\overline{U}}_{2,y}\sin(\widetilde{\overline{U}}_{1,y})\Delta\lambda_{des} - \ldots \\ \ldots - (-1)^{k_1}(-1)^{k_2}(1 - C)W_c\widetilde{\overline{U}}_{1,y}\sin(\widetilde{\overline{U}}_{2,y})\Delta\lambda_{des} \end{pmatrix} \tag{55}$$

$$D = 4\pi\Lambda_c\begin{pmatrix} \widetilde{\overline{U}}_{2,y}\widetilde{\overline{U}}_{3,y}\sin(\widetilde{\overline{U}}_{1,y})(k_2 - k_3) + (-1)^{k_2}\widetilde{\overline{U}}_{1,y}\widetilde{\overline{U}}_{3,y}k_3\sin(\widetilde{\overline{U}}_{2,y}) - \ldots \\ \ldots - (-1)^{k_3}\widetilde{\overline{U}}_{1,y}\widetilde{\overline{U}}_{2,y}k_2\sin(\widetilde{\overline{U}}_{3,y}) \end{pmatrix} \tag{56}$$

where

$$\Theta = \sqrt{\frac{\Delta\delta e_x^2 + \Delta\delta e_y^2}{\Delta\delta e_x^2}} \quad \overline{U} = \text{atan}\left(\frac{\Delta\delta e_{y,des}}{\Delta\delta e_{x,des}}\right). \tag{57}$$

REFERENCES

[1] S.S. Vaddi, K.T. Alfriend, S.R. Vadali, et al., "Formation establishment and reconfiguration using impulsive control". *Journal of Guidance, Control, and Dynamics*. Vol. 28, No. 2, 2005, pp. 262–268, DOI: 10.2514/1.6687.

[2] Y. Ichimura, A. Ichikawa, "Optimal impulsive relative orbit transfer along a circular orbit". *Journal of Guidance, Control, and Dynamics*. Vol. 31, No. 4, 2008, pp. 1014–1027, DOI: 10.2514/1.32820.

[3] M. Chernick, S. D'Amico, "New Closed-Form Solutions for Optimal Impulsive Control of Spacecraft Relative Motion". *AIAA Space and Astronautics Form and Exposition*, SPACE 2016, Long Beach Convention Center California, 13-16 September, 2016.

[4] M. Lawn, G. Di Mauro and R. Bevilacqua, "Guidance solutions for Spacecraft Planar Rephasing and Rendezvous using Input Shaping Control". *27th AAS/AIAA Space Flight Mechanics Meeting, San Antonio*, 2017.

[5] L. Steindorf, S. D'Amico, J. Scharnagl, F. Kempf, K. Schilling, "Constrained Low-Thrust Satellite Formation-Flying using Relative Orbit Elements". *27th AAS/AIAA Space Flight Mechanics Meeting*, San Antonio, Texas, February 5-9, 2017.

[6] Koenig, A.W., Guffanti, T. and D'Amico, S., "New State Transition Matrices for Relative Motion of Spacecraft Formations in Perturbed Orbits," *AIAA/AAS Astrodynamics Specialist Conference, SPACE Conference and Exposition,* AIAA, 2016, DOI: 10.2514/6.2016-5635.

[7] D'Amico, S., "Autonomous Formation Flying in Low Earth Orbit," Ph.D. Dissertation, University of Delft, Delft, Netherlands, 2010.

[8] S. D'Amico, "Relative Orbital Elements as Integration Constants of Hill's Equations," DLR-GNSOC TN 05-08, Oberpfaffenhofen, 2005.

[9] Roscoe, C.W. T., Westphal, J.J., Griesbach, J.D., and Schaub H., "Formation Establishment and Reconfiguration Using Differential Elements in J2-Perturbed Orbits", Journal of Guidance, Control, and Dynamics, Vol. 38, pp. 1725-1740, 2015, DOI: 10.2514/1.G000999.

[10] Schaub, H. and Junkins, J. L., Analytical Mechanics of Space Systems, AIAA, Reston, Virginia (USA), 2014, Chap. 14

[11] J. Sullivan, A. W. Koening and S. D'Amico, "Improved MAneuver Free Approach Angles-Only Navigation for Space Rendezvous," *Advances in the Astronautical Sciences Spaceflight Mechanics,* vol. 158, 2016.

[12] Crassidis and J. L. Junkins, Optimal Estimation of Dynamic Systems, CRC Press, 2004.

[13] D. Brouwer, "Solution of the Problem of Artificial Satellite Theory Without Drag," *Astronautical Journal,* vol. 64, no. 1274, 1959, pp. 378-397.

[14] R. Lyddane, "Small Eccentricities or Inclinations in the Brouwer Theory of the," *Astronomical Journal,* vol. 68, no. 8, 1963, pp. 555-558.

[15] Vallado, D.A., Fundamentals of Astrodynamics and Applications, Springer-Verlag New York, 2007.